Monitoring Metastasis and Cachexia in a Patient with Breast Cancer: A Case Study

Nikita Consul[1], Xiaotao Guo[2], Courtney Coker[3], Sara Lopez-Pintado[4], Hanina Hibshoosh[5], Binsheng Zhao[2], Kevin Kalinsky[6,*] and Swarnali Acharyya[3,*]

[1]Department of Medicine, College of Physicians and Surgeons, Columbia University. [2]Department of Radiology, Columbia University Medical Center, New York, NY, USA. [3]Institute for Cancer Genetics, Herbert Irving Comprehensive Cancer Center, Columbia University, New York, NY, USA. [4]Department of Biostatistics, Mailman School of Public Health, Columbia University, New York, NY, USA. [5]Department of Pathology and Cell Biology, Columbia University Medical Center, New York, NY, USA. [6]Division of Hematology and Medical Oncology, Columbia University Medical Center, New York, NY, USA. *Co-corresponding authors.

ABSTRACT: Cachexia, a wasting syndrome associated with advanced cancer and metastasis, is rarely documented in breast cancer patients. However, the incidence of cachexia in breast cancer is now thought to be largely underestimated. In our case report of a breast cancer patient with bone metastasis monitored during the course of her treatment, we document the development of cachexia by image analysis in relation to her metastatic burden. Elucidation of the link between metastatic burden and cachexia could unveil a highly specific screening process for metastasis, by assessing true muscle mass loss. Our patient was a 49-year-old premenopausal woman, with metastatic invasive ductal breast carcinoma in the vertebral and iliac bones on presentation, which progressed with new metastases to her hips, thigh bones, and vertebrae. In the two-year period, that is between her diagnosis and death, she lost >10% of her baseline weight. During these two years, we retrospectively identified a decrease in paraspinal muscle (PM) at the third lumbar vertebra followed by a sharp decline in weight. The increased tumor burden over time in metastatic sites was accompanied by a decrease in abdominal muscle and visceral and subcutaneous fat and was followed by the patient's demise. The increasing tumor burden in the patient was correlated with the mass of other tissues to determine the tissue that could best serve as a surrogate marker to cachexia and tumor burden. We noted a strong negative correlation between PM area and metastatic tumor area at the third lumbar vertebral level, with PM loss correlating to increasing tumor burden. The monitoring of PM wasting may serve as a marker, and therefore a prognostic factor, for both cachexia and extent of metastatic disease, especially in breast cancer, where metastasis to bone is frequent. Based on our data and review of the literature in this case study, longitudinal monitoring of cachexia in the selected muscle groups can give clinicians early indications of the extent of cachexia in metastatic breast cancer patients.

KEYWORDS: breast cancer, cachexia, radiological quantification, vertebral metastasis, bone metastasis, weight loss

CITATION: Consul et al. Monitoring Metastasis and Cachexia in a Patient with Breast Cancer: A Case Study. *Clinical Medicine Insights: Oncology* 2016:10 83–94 doi: 10.4137/CMO.S40479.

TYPE: Case Report

RECEIVED: June 28, 2016. **RESUBMITTED:** August 08, 2016. **ACCEPTED FOR PUBLICATION:** August 10, 2016.

ACADEMIC EDITOR: William Chi-shing Cho, Editor in Chief

PEER REVIEW: Four peer reviewers contributed to the peer review report. Reviewers' reports totaled 333 words, excluding any confidential comments to the academic editor.

FUNDING: SA is an assistant professor of Avon Products Foundation at Columbia University and a recipient of the Pathway to Independence K99/R00 award (CA172697) and METAvivor award. KK was supported by the National Center for Advancing Translational Sciences, National Institutes of Health, through grant number KL2 TR000081. SA was supported by the start-up funds of Columbia University. The content is solely the responsibility of the authors and does not necessarily represent the official views of the National Institutes of Health. The authors confirm that the funder had no influence over the study design, content of the article, or selection of this journal.

COMPETING INTERESTS: Authors disclose no potential conflicts of interest.

CORRESPONDENCE: sa3141@cumc.columbia.edu

COPYRIGHT: © the authors, publisher and licensee Libertas Academica Limited. This is an open-access article distributed under the terms of the Creative Commons CC-BY-NC 3.0 License.

Paper subject to independent expert blind peer review. All editorial decisions made by independent academic editor. Upon submission manuscript was subject to anti-plagiarism scanning. Prior to publication all authors have given signed confirmation of agreement to article publication and compliance with all applicable ethical and legal requirements, including the accuracy of author and contributor information, disclosure of competing interests and funding sources, compliance with ethical requirements relating to human and animal study participants, and compliance with any copyright requirements of third parties. This journal is a member of the Committee on Publication Ethics (COPE).

Published by Libertas Academica. Learn more about this journal.

Background

Involuntary weight loss seen in several chronic illnesses, such as cancer, is termed cachexia and is distinguished from anorexia by its underlying mechanism. Currently, there is no established consensus for screening patients for cachexia, which can present as fatigue and anorexia, metabolic dysfunction, or systemic inflammation.[1] Cachexia is a loss of >5% of body weight primarily due to the loss of muscle mass with or without adipose tissue loss, while anorexia is due to utilization of adipose stores.[2] The main underlying pathophysiology of cancer cachexia is thought to be the release of tumor cytokines that interfere with host immunity and cause widespread effects called paraneoplastic syndromes.[3–5] Muscle wasting in cachexia may be due to the presence of inflammatory cytokines that cause lipolysis with increased production of brown fat, which causes changes to adipose tissue levels and may present as infiltration of adipose tissue in skeletal muscle, both of which promote increased muscle wasting.[4,6] Few options exist for managing symptoms of cachectic patients, beyond increased nutrition and appetite stimulants, none of which have been shown to decrease muscle wasting.[7] Not surprisingly, cachexia remains a significant predictor of mortality in cancer patients.

Metastasis is believed to be responsible for ~90% of cancer patient deaths,[8,9] and cachexia is found in 50–80% of patients with advanced cancers, largely overlapping with metastatic disease.[3,10,11] Metastasis may increase the paraneoplastic potential of cancer, and cachexia may promote further spread of cancer as the body weakens gradually.[12] This is illustrated by the observation that cancer cachexia is considered an early

complication after diagnosis of gastric or pancreatic cancer, but a late complication following breast or lung cancer diagnosis. Overall, cachexia is associated with the advanced stages of most cancer subtypes.[5,7]

Cachexia has been most prevalent in pancreatic, gastric, colorectal, lung, and head and neck cancers[13] and is not often documented in breast cancer patients. However, recent studies by Waning and Guise have shown that in breast cancer patients, the relationship between metastasis and cachexia may be more complex than originally thought. In fact, cachexia is largely observed in settings with metastases to bony sites that might directly have an effect on muscle, as part of the body's normal musculoskeletal endocrine system.[4,12] By studying the case of a patient with the rare syndrome of cachexia associated with her metastatic breast cancer, we aimed to define characteristics of the cancer–cachexia relationship. We found that increased metastatic breast cancer tumor burden in our patient correlated strongly with a decrease in muscle mass and excess weight loss.

Case Summary

The patient, a 49-year-old premenopausal woman, was admitted to the emergency department in August 2013 with persistent, severe, cramping back pain, but otherwise in good health. Her symptoms began in May 2013, when she felt as if her "rib broke" during a sneeze, and in June 2013, she had a normal chest X-ray. She was put on cyclobenzaprine, naproxen, and physical therapy, but after a long flight in July 2013, she felt as if she "threw out her back" while getting up. The back pain was now only manageable with narcotics and was accompanied by urinary and fecal urgencies. On workup at the emergency department, a chest X-ray was notable for a new thoracic vertebral compression fracture not seen two months prior. A follow-up computational tomography (CT) imaging revealed diffuse lytic lesions throughout the lumbar spine, sacrum, and ilium, which were read as concerning for metastases or myeloma with no evidence of intrathoracic, intra-abdominal, or intrapelvic malignancy.

In light of possible metastases, the patient was admitted to the oncology service. Physical examination revealed slight retraction of the right nipple, with subjective increased density of the right breast tissue as compared to the left breast; otherwise, the examination was within normal limits. Serum laboratory tests showed elevated calcium (11.6 mg/dL), albumin (4.0 g/dL), and a mildly elevated alkaline phosphatase (136 mg/dL). Magnetic resonance imaging (MRI) of the thoracic and lumbar spine revealed tumor within the eleventh thoracic (T11) vertebral body, leading to moderate spinal canal stenosis, with epidural enhancement extending from the inferior tenth thoracic level to the superior twelfth thoracic (T12) level and neoplastic extension anteriorly immediately adjacent to the posterior aorta. Diffuse tumor was identified in all lumbar vertebrae, multiple adjoining ribs, and iliac bones. Follow-up mammography revealed a "highly suspicious" sonographic and mammographic abnormality of up to 6 cm at 9:00 in the right upper-outer breast, composed of fine pleomorphic calcifications, scoring 5 on the Breast Imaging Reporting and Data System scale.

The breast was explored as the potential primary site of the cancer. Right breast core biopsy at 9:00 showed a moderately differentiated invasive ductal carcinoma (IDC) that was estrogen receptor positive (ER+), progesterone receptor positive (PR+), and human epidermal growth factor receptor 2 negative (HER2–), with a Ki67 score of 25% (Table 1A), consistent with stage IV breast cancer. No germline mutations were identified. CT-guided core biopsy of the right iliac bone revealed metastatic IDC that was ER+, PR–, and HER2–, with a Ki67 score of 10% (Table 1A). Representative images of the IDC in both the right breast and right hip are shown in Figure 1A and B. The patient underwent a laparoscopic bilateral salpingo-oophorectomy, which was histologically unremarkable.

In September 2013, she was enrolled in a phase III trial of letrozole, an aromatase inhibitor, and palbociclib, a cyclin-dependent kinase 4/6 inhibitor, versus letrozole and placebo. She received infusion regularly to manage hypercalcemia. In November 2013, she began to notice weight loss and decreased appetite, for which she was referred to nutrition services. She continued through 19 cycles of chemotherapy, with 95–100% compliance to the therapeutic regimen, before exiting the study in the middle of her 20th cycle in late March 2015, in view of disease progression. She was unblinded and determined to be receiving palbociclib and not placebo. The breast mass size over the course of chemotherapy is presented in Table 1B.

In January 2015, she began to complain of left hip pain "like nerve pain" radiating down to the knee, with CT showing diffuse lytic intraosseous metastases, with no new femur lesions discernable. MRI showed no displaced pathologic fracture at the time, but repeat MRI in March 2015 demonstrated progression of diffuse metastatic disease, new moderate T2 compression fracture, severe T11 compression fracture, new cord T2 signal hyperintensity, and multilevel epidural disease from T11 to the first lumbar (L1) vertebra, involving foramina of T11–T12. Neurosurgery led to decompression of spinal cord and stabilization. A subsequent left displaced femoral neck fracture was addressed with a left total hip replacement. Histology of the femur revealed metastatic IDC (Fig. 1C).

Table 1A. Tumor characteristics. Tumor was biopsied at the primary site and at metastatic sites. The tumor was found to be representative of invasive ductal breast carcinoma at all sites. See Figure 1.

SAMPLE	ER	PR	Her2	Ki67
R Breast (primary tumor)	+	+	–	25%
R iliac spine (first metastasis)	–	–	–	10%

Table 1B. Tumor size at the primary site. Throughout the course of treatment, the tumor burden at the primary site decreased, while the number of metastases increased. The breast mass size was measured by a caliper for width along the longest axis at regular clinical visits.

DATE	WIDTH (CM)
11/22/13	3.3
1/17/14	2.8
2/14/14	2.7
3/14/14	2.7
4/9/14	2.6
5/7/14	2.4
6/4/14	2.0
7/2/14	2.0
7/30/14	1.4
8/27/14	1.5
9/17/14	1.5
10/22/14	1.3
11/19/14	1.3
12/17/14	1.0
1/14/15	1.0
2/11/15	1.0
3/11/15	1.0

Her course was notable for further weight loss, a right femoral neck fracture, and total hip replacement surgery in May 2015 and a surgical wound opening in July 2015 that was complicated with an emergent thoracic spine wound revision and postoperative vancomycin/cefepime. She died in September 2015, likely due to a pulmonary embolus, despite being on full-dose anticoagulation. The patient's weight loss was a significant marker of the severity of disease. Her weight loss over time could have been affected by clinical events, medical intervention, or surgical intervention (Fig. 2).

The mechanisms of muscle and fat loss in cancer are not yet well elucidated and may in fact be interrelated with the development of new metastases in advanced stages of cancers. We note, with interest, potential correlations among the growth of our patient's metastatic tumor burden and her cachexia, by quantifying changes over time in the cross-sectional area of the following five tissue types at the third lumbar (L3) vertebral axial level: tumor metastases at the vertebral spine (TU), subcutaneous fat (SF), visceral fat (VF), abdominal muscle (AM), and paraspinal muscle (PM).

Methods

Histology. Biopsy tissues were fixed in 10% buffered formalin, paraffin embedded, and cut into 5 μm sections on a Leica microtome. The sections were stained with Gill's hematoxylin, bluing agent, and alcoholic eosin Y at the Herbert Irvine Comprehensive Cancer Center's molecular shared resource at the Columbia University Medical Center (Acharyya 2012)[14] (Fig. 1). Histological analysis of all biopsy samples was performed by a pathologist (Table 1A).

Radiological quantification: cross-section at L3 vertebra. TU (Fig. 3A), AM (Fig. 3B), and PM (Fig. 3C) cross-sectional areas were quantified within axial images of serial CT abdomen/pelvis scans at a superior and an inferior L3 vertebral level. The total area quantification in millimeter squared was made at both sub levels with automated tissue segmentation software based on differential Hounsfield units across user-created contours, designed by Zhao et al at the Columbia University's Computational Imaging Analysis Laboratory. These two numbers were averaged for an average cross-sectional area across the L3 vertebral level.

The cross-sectional areas of SF and VF were quantified from images of serial CT abdomen/pelvis scans at a superior and at an inferior L3 vertebra level using a fat segmentation software (Zhao 2006)[15] that separated SF from VF by the user-demarcated AM boundary (Fig. 3D). The superior and inferior values for each scan were averaged for an L3 estimate at that timepoint.

Pearson's (r) and Spearman's (ρ) coefficients were calculated for correlations among each of the tissue types for the raw cross-sectional area data. Correlation matrices were generated with these coefficients (Tables 2 and 3). Different

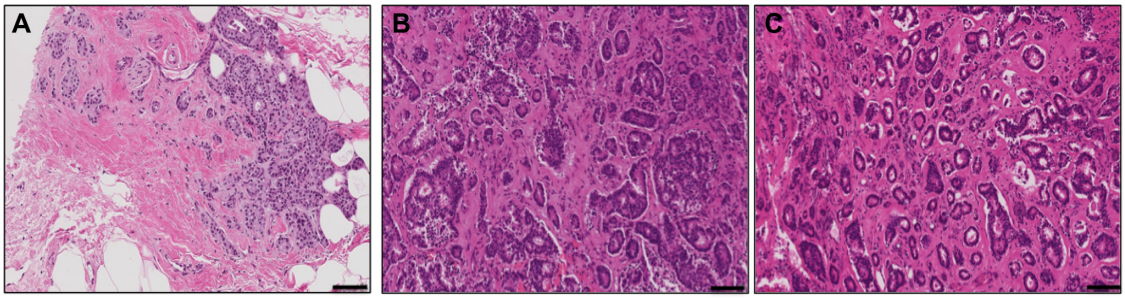

Figure 1. H&E images of breast tumor and bone metastasis. (**A**) Shows well-differentiated to moderately differentiated invasive ductal breast carcinoma in the right breast. (**B–C**) Shows metastasis with well-differentiated features of invasive ductal breast carcinoma isolated from the hip (**B**) and femur (**C**) resection from the same patient. Scale bar represents 100 μm.

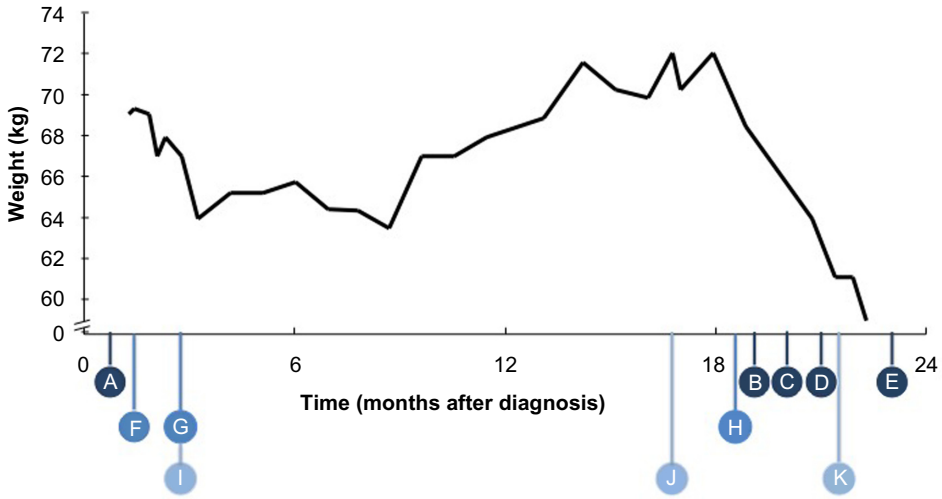

Figure 2. Weight versus time (months after diagnosis) and surgical, pharmacological, and clinical events. An initial decrease in weight corresponds with the initiation of surgical and medical interventions; later a decline in weight around 18 months after the time of diagnosis in August 2013 corresponds with the timing of several interventions and clinical events. Lettered items below the axis in dark blue correspond to surgical events as follows: A) bilateral salpingo-oophorectomy, B) spinal fusion, C) right total hip replacement, D) left total hip replacement, and E) wound spinal revision. Lettered items below the axis in bright blue correspond to clinical events as follows: F) start letrozole, G) start Arixta, and H) stop letrozole. Lettered items below the axis in pale blue correspond to clinical events as follows: I) left deep vein thrombosis, J) left femur and left hip metastasis, and K) right hip, right femur metastasis, and T11 metastasis.

timescales were used for the tissue types, as compared to the tumor burden, to assess for possible lag in time that may delay a change in one tissue with respect to the change in another tissue type (Table 4). Conditional formatting for the highest values in pale yellow and the lowest values in bright green was applied for green-to-yellow coloration using Microsoft Excel to observe for associations between the outcomes of different tissue types.

Results

Histology. Breast tissue biopsy from the right breast revealed well-differentiated to moderately differentiated IDC

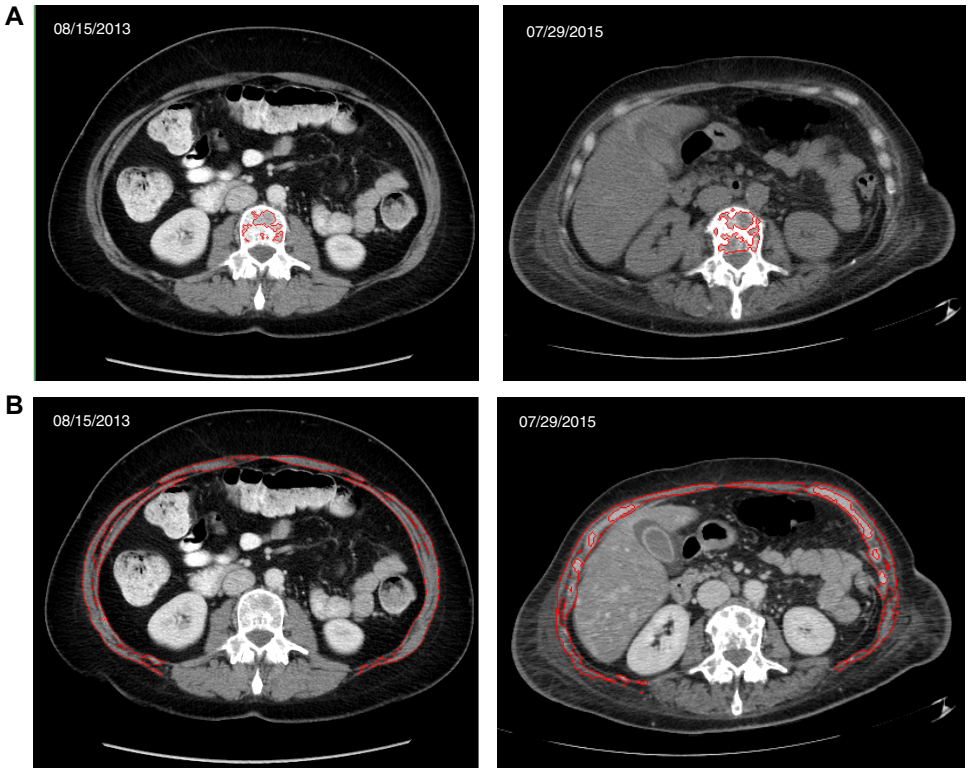

Figure 3. (*Continued*)

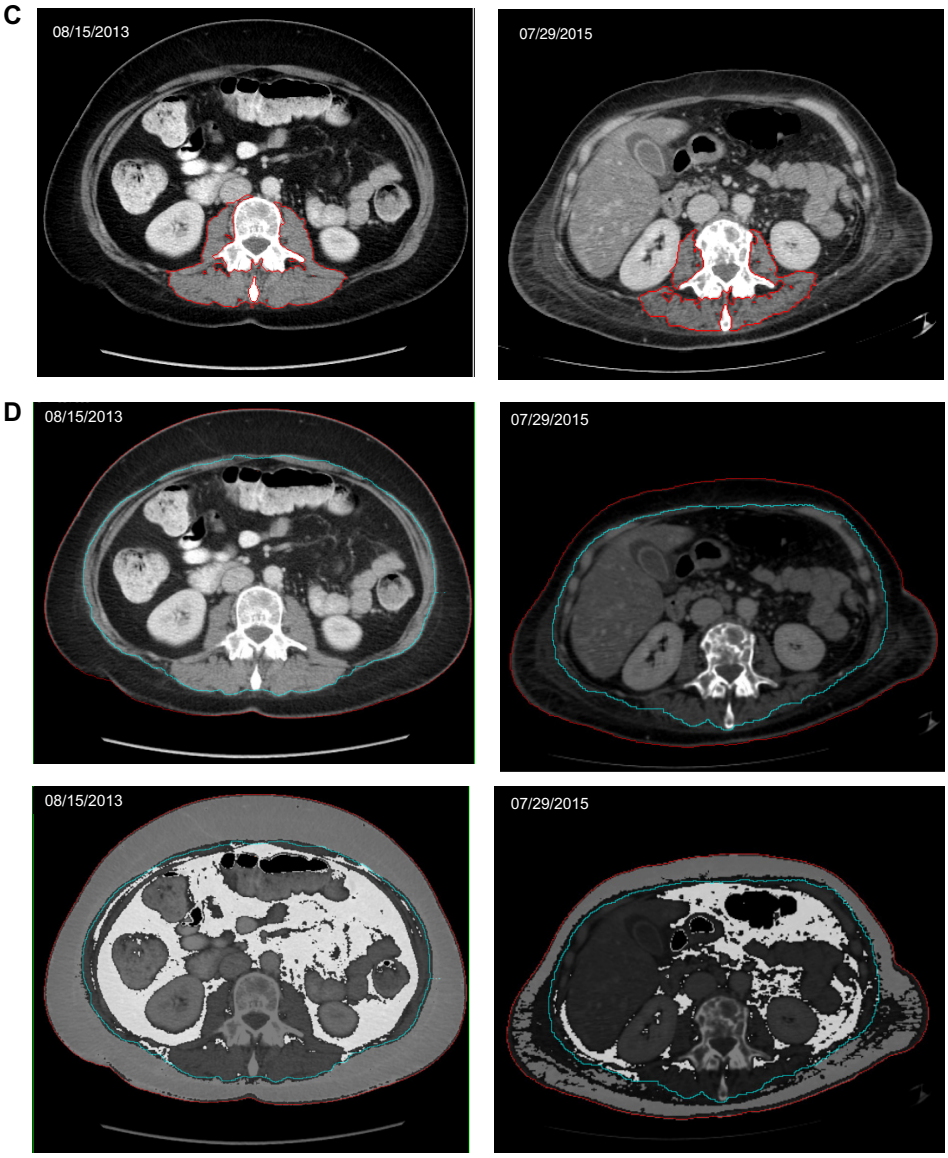

Figure 3. (**A**) TU segmentation. CT abdomen/pelvis scan image at the L3 vertebral level. (**B**) AM segmentation. CT abdomen/pelvis scan image at the L3 vertebral level. (**C**) PM segmentation. CT abdomen/pelvis scan image at the L3 vertebral level. (**D**) Fat segmentation with top row of figures showing segmentation contours, and bottom row showing coloration of VF within the teal contour and SF between the red and teal contours. CT abdomen/pelvis scan image at the L3 vertebral level.

consistent with the previously mentioned clinical diagnosis (Fig. 1A). Tissue samples from the hip (Fig. 1B) and femur (Fig. 1C) revealed metastases of the breast carcinoma in the skeletal sites.

Radiological quantification: cross-section at L3 vertebra. Tumor tissue segmentation revealed an overall increase in TU from August 15, 2013, to July 29, 2015 (Fig. 3A), while AM and PM segmentations revealed an overall decrease from August 15, 2013, to July 29, 2015 (Fig. 3B and C, respectively). Fat segmentation and segregation into VF and SF also revealed an overall decrease in both SF and VF from August 15, 2013, to July 29, 2015 (Fig. 3D). Plotted over time, measurements of cross-sectional tissue areas revealed opposing trends in the areas of PM, AM, VF, and SF versus the area of TU (Fig. 4A and B), further investigated with correlation analysis. Correlation matrices of r are shown in Table 2A–F, and correlation matrices of ρ are shown in Table 3A–F. The matrices were built to show correlation coefficients of 1.00 when a tissue type is correlated with itself. Correlations among the raw cross-sectional areas of the five tissue types generally showed weak positive correlations among SF, VF, AM, and PM, but showed moderate-to-strong negative correlations when any of SF, VF, AM, or PM was correlated with TU.

SF versus TU. SF correlated strongly negatively against TU with $r = -0.65$ (Table 2A), $r = -0.64$ (Table 2B), $r = -0.70$ (Table 2E), $\rho = -0.54$ (Table 3B), and $\rho = -0.63$ (Table 3E). Negative correlations for SF and TU, with SF at the lagging timepoint compared to TU, indicates that decreases in SF proceeded after a time lag following increases in TU in our case study patient (Table 4). This corresponds with the visual

Table 2. Pearson's correlations (*r*) among all tissue types: TU, SF, VF, AM, and PM. A box in the table holds the value of *r* that corresponds to the data for the two tissue types corresponding with the row and column assigned to that box. The strongest hue of green indicates a more negative correlation, while the weakest hue (pale yellow) indicates a more positive correlation. Looking at green colorations, the strongest negative correlations seem to exist between TU and another tissue type, along the first row or the first column. (**A**) Represents correlations for the cross-sectional raw areas as they were quantified and recorded. TU and VF are the most negatively correlated, with moderate negative correlations of the other tissues against TU. (**B**) Represents correlations for areas of TU at the timepoint *t* against the areas of the other four tissue types at the timepoint $t + 1$. This shows that SF against TU and VF against TU are most strongly negatively correlated. (**C**) Represents correlations for areas of TU at the timepoint *t* against the areas of the other four tissue types at the timepoint $t - 1$. VF against TU and PM against TU are negatively correlated, with a moderate positive correlation of AM against PM and SF against VF. (**D**) Represents correlations among the incremental gains in the area for each tissue type during an interval between the same timepoints. Here, there is a strong negative correlation of AM against TU. (**E**) Represents the correlation between the incremental gain in the area for TU at the timepoint *t* against the incremental gain in areas for the other four tissue types at the timepoint $t + 1$. This shows a strong negative correlation of SF against TU and a moderate negative correlation of VF against TU, with a moderate positive correlation of AM and PM against TU. (**F**) Represents the correlation between the incremental gain in the area for TU at the timepoint *t* against the incremental gain in areas for the other four tissue types at the timepoint $t - 1$. There is a strong negative correlation of VF and PM against TU, with a moderate negative correlation of SF against TU.

A	TU	SF	VF	AM	PM
TU	1.00	−0.65	−0.71	−0.39	−0.70
SF	−0.65	1.00	0.81	0.14	0.56
VF	−0.71	0.81	1.00	0.12	0.48
AM	−0.39	0.14	0.12	1.00	0.44
PM	−0.70	0.56	0.48	0.44	1.00

B	TU	SF	VF	AM	PM
TU	1.00	−0.64	−0.56	0.16	−0.26
SF	−0.64	1.00	0.81	0.17	0.55
VF	−0.56	0.81	1.00	0.19	0.41
AM	0.16	0.17	0.19	1.00	0.52
PM	−0.26	0.55	0.41	0.52	1.00

C	TU	SF	VF	AM	PM
TU	1 00	−0.17	−0.52	−0.13	−0.83
SF	−0 17	1.00	0.63	−0.31	0.28
VF	−0 52	0.63	1.00	−0.21	0.20
AM	−0.13	−0.31	−0.21	1.00	0.28
PM	−0.83	0.28	0.20	0.28	1.00

D	TU	SF	VF	AM	PM
TU	1.00	−0.17	−0.09	−0.71	−0.20
SF	−0.17	1.00	0.69	−0.11	0.04
VF	−0.09	0.69	1.00	−0.01	−0.01
AM	−0.71	−0.11	−0.01	1.00	0.33
PM	−0.20	0.04	−0.01	0.33	1.00

E	TU	SF	VF	AM	PM
TU	1.00	−0.70	−0.24	0.49	0.28
SF	−0.70	1.00	0.69	−0.12	0.17
VF	−0.24	0.69	1.00	−0.01	0.06
AM	0.49	−0.12	−0.01	1.00	0.35
PM	0.28	0.17	0.06	0.35	1.00

F	TU	SF	VF	AM	PM
TU	1.00	−0.22	−0.66	−0.04	−0.53
SF	−0.22	1.00	0.64	−0.14	0.30
VF	−0.66	0.64	1.00	−0.01	0.12
AM	−0.04	−0.14	−0.01	1.00	0.35
PM	−0.53	0.30	0.12	0.35	1.00

representation of SF over time peaking at timepoints after the troughs in TU over time, and vice versa (Fig. 4B).

VF versus TU. VF correlated strongly negatively against TU with $r = -0.71$ (Table 2A), $r = -0.56$ (Table 2B), $r = -0.52$ (Table 2C), $r = -0.66$ (Table 2F), $\rho = -0.56$ (Table 3C), and $\rho = -0.62$ (Table 3F). Negative correlations for VF and TU, with VF at the timepoint preceding TU, indicates that decreases in VF preceded increases in TU that followed after a time lag, and vice versa (Table 4). This corresponds with the graph of VF over time peaking at timepoints just prior to the troughs in TU (Fig. 4B).

AM versus TU. AM correlated strongly negatively against TU with $r = -0.71$ (Table 2D) and $\rho = -0.71$ (Table 3D). AM also correlated moderately positively against TU with $r = 0.49$ (Table 2E) and $\rho = -0.27$ (Table 3E). Correlations between AM and TU were strongly negative when the incremental change in AM was compared to the incremental change in TU between the same two timepoints, but were moderately positive when the incremental change in AM at a lagging timepoint was correlated with TU incremental change at a preceding timepoint (Table 4). This may indicate a closely inverse relationship at some timepoints between the growth in AM and the growth in TU for our case study patient, which corresponds with the graph representations of AM and TU over time (Fig. 4B).

PM versus TU. PM correlated strongly negative against TU with $r = -0.70$ (Table 2A), $r = -0.83$ (Table 2C), $r = -0.53$ (Table 2F), $\rho = -0.55$ (Table 3C), and $\rho = -0.55$ (Table 3F). Negative correlations between PM and TU were strong when PM at the preceding timepoint was compared to TU at the following timepoint, indicating that changes in PM preceded the inverse change in TU that followed after a time lag, and vice versa (Table 4). This corresponds with the graph of PM following an overall decrease over time, while TU increased overall. Notably, PM experienced few increases throughout its growth over the two-year period assessed, while other tissue

Table 3. Spearman's correlations (ρ) among all tissue types: tumor, SF, VF, AM, and PM. A box in the table holds the value of the Spearman's correlation coefficient that corresponds to the data for the two tissue types corresponding with the row and column assigned to that box. The strongest hue of green indicates a more negative correlation, while the weakest hue (pale yellow) indicates a more positive correlation. Looking at green colorations, the strongest negative correlations seem to exist between TU and another tissue type, along the first row or the first column. (**A**) Represents correlations for the cross-sectional raw areas as they were quantified and recorded. TU and VF are the most negatively correlated, with moderate negative correlations of the other tissues against TU. (**B**) Represents correlations for areas of TU at the timepoint *t* against the areas of the other four tissue types at the timepoint $t + 1$. This shows SF against TU is the most strongly negatively correlated. (**C**) Represents correlations for areas of TU at the timepoint *t* against the areas of the other four tissue types at the timepoint $t - 1$. VF against TU and PM against TU are negatively correlated, with a moderate positive correlation of AM against PM and SF against VF. (**D**) Represents correlations among the incremental gains in the area for each tissue type during an interval between the same timepoints. Here, there is a strong negative correlation of AM against TU. (**E**) Represents the correlation between the incremental gain in the area for TU at the timepoint *t* against the incremental gain in areas for the other four tissue types at the timepoint $t + 1$. This shows a strong negative correlation of SF against TU and a moderate negative correlation of VF against TU, with a moderate positive correlation of AM against TU. (**F**) Represents the correlation between the incremental gain in the area for TU at the timepoint *t* against the incremental gain in areas for the other four tissue types at the timepoint $t - 1$. There is a strong negative correlation of VF and PM against TU, with a moderate negative correlation of SF against TU.

A	TU	SF	VF	AM	PM
TU	1.00	−0.29	−0.47	−0.28	−0.38
SF	−0.29	1.00	0.67	0.02	0.27
VF	−0.47	0.67	1.00	0.05	0.19
AM	−0.28	0.02	0.05	1.00	0.40
PM	−0.38	0.27	0.19	0.40	1.00

B	TU	SF	VF	AM	PM
TU	1.00	−0.54	−0.37	0.13	−0.10
SF	−0.54	1.00	0.66	0.01	0.24
VF	−0.37	0.66	1.00	0.15	0.12
AM	0.13	0.01	0.15	1.00	0.50
PM	−0.10	0.24	0.12	0.50	1.00

C	TU	SF	VF	AM	PM
TU	1.00	−0.18	−0.56	−0.05	−0.55
SF	−0.18	1.00	0.56	−0.31	0.08
VF	−0.56	0.56	1.00	−0.26	−0.05
AM	−0.05	−0.31	−0.26	1.00	0.21
PM	−0.55	0.08	−0.05	0.21	1.00

D	TU	SF	VF	AM	PM
TU	1.00	−0.25	−0.16	−0.71	−0.15
SF	−0.25	1.00	0.72	0.12	−0.01
VF	−0.16	0.72	1.00	−0.08	−0.14
AM	−0.71	0.12	−0.08	1.00	0.18
PM	−0.15	−0.01	−0.14	0.18	1.00

E	TU	SF	VF	AM	PM
TU	1.00	−0.63	−0.38	0.27	0.13
SF	−0.63	1.00	0.78	0.20	0.12
VF	−0.38	0.78	1.00	−0.07	−0.18
AM	0.27	0.20	−0.07	1.00	0.13
PM	0.13	0.12	−0.18	0.13	1.00

F	TU	SF	VF	AM	PM
TU	1.00	−0.30	−0.62	−0.05	−0.55
SF	−0.30	1.00	0.70	0.02	0.22
VF	−0.62	0.70	1.00	−0.08	0.02
AM	−0.05	0.02	−0.08	1.00	0.37
PM	−0.55	0.22	0.02	0.37	1.00

types experienced remarkable increases and decreases over time (Fig. 4B).

In summary, VF and PM correlate negatively with TU when TU is measured at a lagging timepoint, AM correlates negatively or positively with TU depending on how they are compared across time, and SF correlates negatively with TU when assessed at a lagging timepoint as compared to TU.

Discussion

While cancer-related cachexia is commonly attributed to decreased appetite and chemotherapy side effects, it may correlate strongly with clinical events and/or therapeutic interventions. Our patient's advanced breast cancer was associated with severe cachexia, which raises the possibility that cachexia is more common than appreciated in many advanced breast cancer patients.

The true incidence of cancer cachexia is likely to be greatly underestimated in many cancers, including breast.[7] Recent estimates report that, while metastasis is responsible for ~90% of cancer-related deaths,[10] cachexia affects 80% of patients with advanced cancers[11] and is thought to be responsible for 20–40% of cancer deaths.[7] Several factors could contribute to its underestimation, including its variable presentation and multifactorial etiologies. In a study of 8541 patients diagnosed with cancer in 1999–2004,[7] 2.5% were written for the ICD-9 code 799.4 for cachexia, but after retrospective investigation, 23% (1975 patients) of the cancer patients met the definition of cachexia, which had not been diagnosed in 20%. Moreover, 25% of the study population had breast cancer and 27% of the 1975 patients with cachexia had breast cancer. This represents a proportion strikingly close to the overall prevalence of breast

Table 4. Visual representation of various timelines across which correlations were made. A description of the timepoint at which the tissue type (SF, VF, AM, PM) was used in a correlation with TU at the timepoint *t* is provided in the first column, with the corresponding correlation matrices listed in parentheses. A visual representation of the timeline shows when a tissue type (in blue) was measured and when TU (in red) was measured, before they were correlated to generate the correlation matrices in Tables 2 and 3.

Timeline Type	Representation
Tissue and TU at the same timepoint (***Table 2.A.***, ***Table 3.A.***)	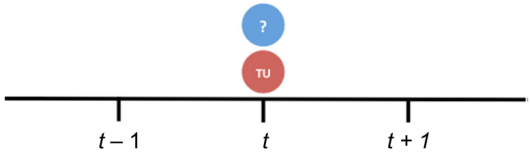
Tissue lags behind TU (***Table 2.B.***, ***Table 3.B.***)	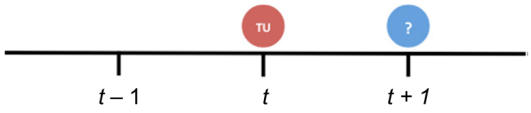
TU lags behind tissue (***Table 2.C.***, ***Table 3.C.***)	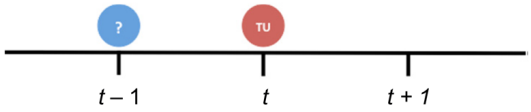
Incremental change of tissue and TU at the same timepoint (***Table 2.D.***, ***Table 3.D.***)	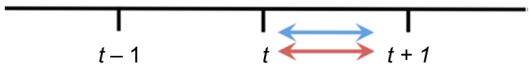
Incremental change for tissue at timepoint lagging behind TU (***Table 2.E.***, ***Table 3.E.***)	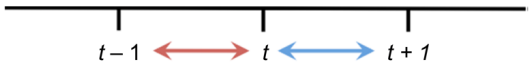
Incremental change for TU at timepoint lagging behind tissue (***Table 2.F.***, ***Table 3.F.***)	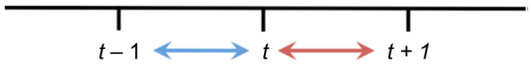

cancer among the patients considered in the study (27% and 25%, respectively).[7]

Several factors may lend to the underdiagnosis of cachexia in all cancer patients, especially with cancer subtypes that follow a slower or more indolent course. While there remains a lack of a consensus definition of cachexia (Blum 2011),[16] routine assessment of patient muscle loss in comparison to overall weight loss provides insight into the presence of cachexia. Of note, no such routine assessment is made consistently with all cancer patients, though cachexia is considered a "landmark of cancer," especially in its late stages.[7] This could be explored in cachexia animal models, as studies exploring the link between prognostic factors and viable treatments in patients are limited due to a lack of approved effective treatment strategies. A decrease in body mass index or weight was strongly inversely related to survival, in a study by Martin et al, of 8160 cancer patients (Martin 2014).[17] Moreover, even if an early diagnosis is made for cachexia, few treatment options exist, with no approved treatments showing significant reversal of cachexia. However, these treatments might temporarily assuage the symptoms of anorexia, weight loss, and insulin resistance,[7] further supported by later studies showing that loss of muscle function in cachexia can occur without overt weight loss.[4,12]

Although cachexia often occurs in advanced cancer stages associated with metastasis, their potential relationship is not well elucidated. Again, there is a need for greater analysis of cachexia in the existing preclinical mouse models of breast cancer metastasis, given the scarcity of animal models for cancer cachexia investigated in the current literature. Mouse models with micro-CT analysis provides for a robust measurement tool for determining the adipose tissue and muscle mass in longitudinal studies without invasive experiments in patients.[18,19] In combination with other imaging modalities such as positron emission tomography and other functional imaging, metastatic lesions can be quantified with

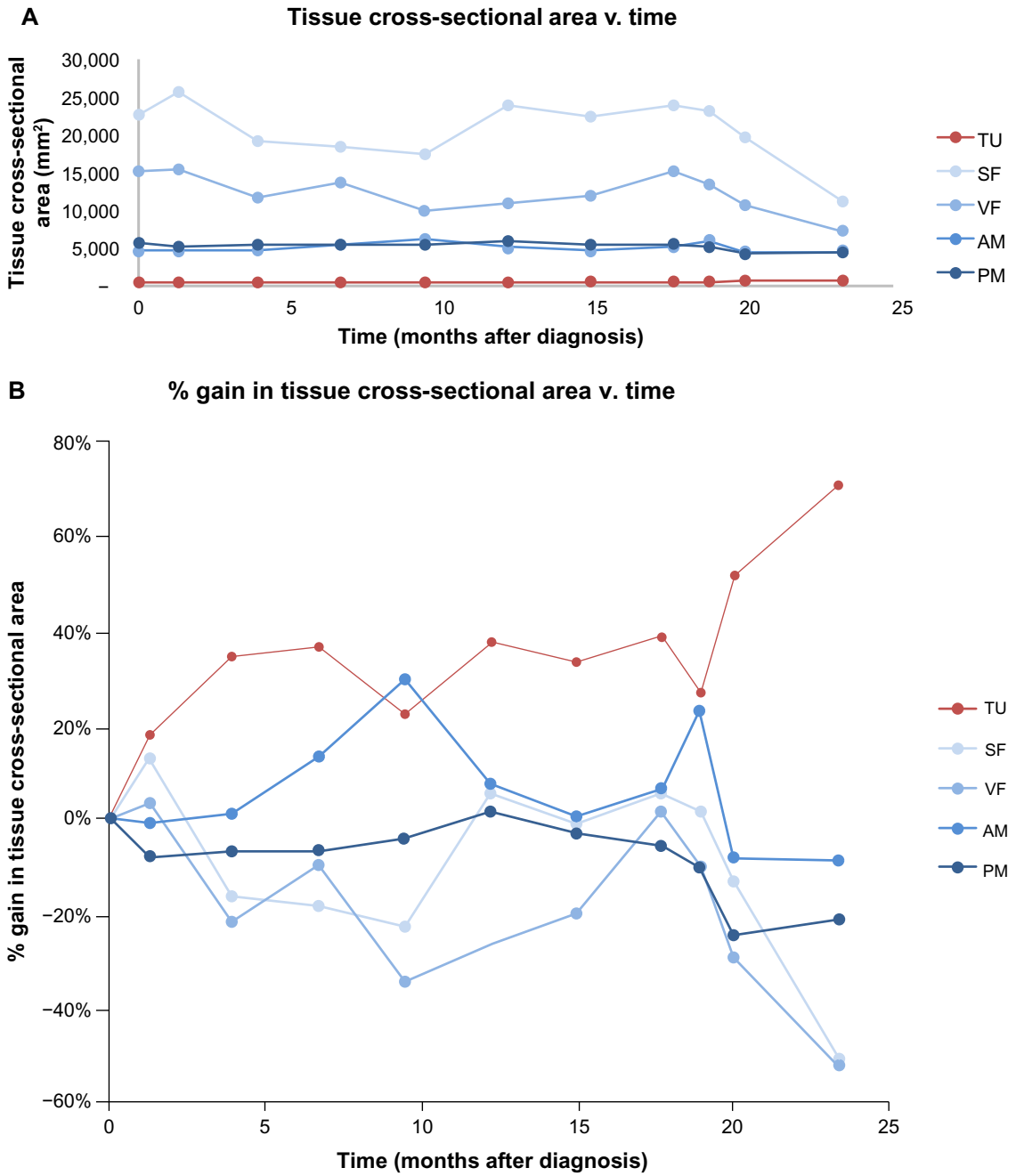

Figure 4. (**A**) Tissue cross-sectional area versus time. Comparing multiple different types of tissue growth (TU, SF, VF, AM, and PM) over time reveals potential trends when normalized to percent gain; while when utilizing raw data, trends are more difficult to see as each tissue cross-sectional area is on a different order of magnitude of scale. (**B**) Percentage gain in tissue cross-sectional area versus time. Comparing multiple different types of tissue growth (TU, SF, VF, AM, and PM) over time reveals potential trends when normalized to percent gain; while when utilizing raw data, trends are more difficult to see as each tissue cross-sectional area is on a different order of magnitude of scale.

high spatial resolution.[20] These measurements and imaging studies could provide us with important insights into the kinetics of cachexia in the context of systemic metastasis and treatment.

In our case study, at 15 months after diagnosis, though our patient's overall body weight remained above baseline and stable, metastasis continued to progress (Fig. 2), with a continued decrease in PM loss (Fig. 3). This was followed by a sharp decline in weight and finally recurrent disease modeled by increased tumor burden with a decrease in the total area of SF, VF, AM, and PM, eventually followed by death (Fig. 3). These data are in line with the findings of Baracos et al.[21] in 441 non-small-cell lung cancer patients that showed muscle loss with or without fat loss to be prevalent across all body mass index categories, and therefore having the potential to affect weight variably, while persisting as a common factor across all patients with progressive advanced stages of cancer.

In our case study, the increasing tumor burden at L3, associated with advanced cancer stage, was correlated with the area of other tissues at L3. This was done in order to highlight differences in muscle and fat loss in a cachectic patient, as well as evaluate for which muscle type may decrease as tumor burden increases. Interestingly, the correlation between PM and TU at L3 is moderately negatively correlated when the change in PM at a timepoint $t-1$ is compared to TU at a timepoint t, meaning any change in TU tended to correlate moderately with the change in PM that occurred at the previous timepoint (Tables 2C and F and 3C and F). Compared to SF, VF, and AM, also negatively correlated with TU across different timelines, PM was noted to be more continuously decreasing, while other tissue types seemed to fluctuate in their cross-sectional areas. Given that these are assumptions gleaned from correlative data from a single patient, causal relationships cannot be concluded, and extrapolations to all breast cancer patients are unfounded. Furthermore, we cannot rule out that other factors might have led to comorbidities, such as chemotherapy causing anorexia that led to weight loss. However, the relative time course of each of the five tissue areas in our case patient, at the L3 cross-section, is indeed illustrative of interrelationships that could be investigated in future controlled studies with multiple patients.

Imaging quantifications suggest that the strongest negative Pearson's correlation among our patient's five tissue types was between the area of PM at a preceding timepoint and the area of TU, correlated with $r=-0.83$ (Table 2C), while the strongest negative Spearman's correlation was between the incremental changes in the area at a specific timepoint of AM and TU, correlated with $\rho=-0.71$ (Table 3D). SF and TU were strongly negatively correlated with SF at a lagging timepoint, and VF and TU were strongly negatively correlated with VF at a preceding timepoint. These findings indicate that the mechanisms behind VF loss and PM loss may proceed more rapidly than those that govern the increase in TU. The SF loss, on the other hand, may likewise occur due to a slower mechanism than that of the mechanism behind increasing TU. Finally, AM loss and increasing TU burden may arise due to similar factors or correlate randomly due to other related factors.

Based on our findings, we considered whether PM loss may be correlated with progressive bone metastasis. The continuous decline in PM in light of increasing and fluctuating TU best matches the course of cachexia as it is currently understood as a metabolic phenomenon that is irreversible, unlike anorexia. Waning and Guise suggested that tumor growth in bone induces the release of bone-derived growth factors that may then act systematically to reduce muscle mass, reduce muscle function, and cause muscle weakness.[4] Together, these results suggest an association of metastatic disease tumor burden with muscle loss. In addressing the high correlation of weight versus SF, one must consider that fat in the body fluctuates more rapidly in response to external factors than muscle content and can therefore contribute more dramatically to weight. In contrast, muscle loss may be less directly correlated with muscle mass due to differences in proximity to sites of bone metastases, yet related to the extent of boney metastasis.[5] The AM parameters were seen to correlate strongly with weight, which could be an artifact of fat correlation with weight. Myosteatosis was radiologically evident in the AM, and therefore, an increase in weight that could be due to an increase in fat content may appear to be correlated with the corresponding rise in the AM width. Meanwhile, the continuous decline in PM could describe an underlying relationship between muscle mass and the adjacent site of bony metastatic bone disease.

In breast cancer, bone is the most common site of metastasis. Osteolytic boney lesions arise due to an imbalance in osteoclast-versus-osteoblast activity and are associated with cause pain, increased risk of fracture, and muscle weakness and fatigue.[12] This fatigue and muscle weakness, associated with cancer cachexia, may be due to the coupled nature of muscle and bone anabolism/catabolism effects, due to paracrine and endocrine signals between muscle cells and bone factors.[12] One such signaling molecule transforming growth factor beta (TGF-β), a potent regulator of wound healing in muscle, has been shown to impair myocyte differentiation and is overexpressed with osteolytic lesions. Similarly, calcitriol, a well-known bone differentiation signaling factor that is downregulated in osteolysis secondary to hypercalcemia, could influence muscle function.[12] Yet another mediator, parathyroid hormone-related protein (PTHrP), released in breast cancer, may aid in its metastasis to the bone by promoting osteolysis that induces release of TGF-β.[4] Therefore, PTHrP may have a direct effect on muscle function and mass by inducing osteolysis[4] and by inducing uncoupling of electron transport from mitochondrial membranes to cause a negative energy balance.[4,6,22] Therefore, with PTHrP being a common paraneoplastic syndrome of breast cancer, this may suggest an important mechanism for breast cancer-associated cachexia, representing a higher potential for cachexia to arise in cases of breast cancer than previously assumed.

Given the influential role of cachexia in the clinical presentation of our breast cancer patients, yet low documentation thereof, it is important to overcome the problem of its underdiagnosis in clinical practice. Early diagnosis of cachexia via careful monitoring of muscle wasting, perhaps through routine radiological studies, could allow for earlier intervention and therefore prevention of energy deprivation. Furthermore, recognizing the interrelationship between muscle wasting and tumor metastasis to the skeletal system as an important mechanism behind the rise of cachexia in breast cancer, is a step toward building new methods for early diagnosis of metastasis. In a review of the Waning et al study, Guttridge[5] pointed out that it would be beneficial to build cohorts to study the levels

of possible cachectic molecular factors in multiple types of cancer patients with bone metastases, one example of how studies of cachectic factors in cancer patients with bone metastases could be planned in the future. Moreover, distinguishing the muscle group most closely associated with tumor metastasis to the bone could provide for an improved method of detecting metastasis with high sensitivity and high specificity.

Given that this is a reported case, further studies with a larger cohort of patients could further reveal whether the correlations we have delineated between PM and TU in a single-case study persist across the subpopulation of breast cancer patients. In such studies, important physiological comorbidities that could be confounders for cachexia, including kidney disease, heart disease, chronic obstructive pulmonary disease, and age-related sarcopenia, could be evaluated against metastatic breast cancer as inducers of atrophy in PM. Additionally, a comparison could be made between changes in PM mass and other muscle mass changes to test for specificity. The pathological extent and burden of metastases in all cancer patients considered need to be evaluated against the value of PM loss in breast cancer patients with metastases to other organs. With further understanding of the relationship between muscle mass and physiological versus pathological extent of metastatic disease, monitoring muscle mass changes with imaging studies could allow for earlier detection of new metastatic sites.

Conclusion

While cancer-related cachexia is commonly attributed to decreased appetite and chemotherapy side effects, it is rarely correlated directly with clinical events or interventions. Our patient's advanced breast cancer was associated with severe cachexia, considered to be a rare combination in breast cancer. Based on our data and review of the literature in this case study, longitudinal monitoring of cachexia in selected muscle groups can give clinicians early indications of the extent of cachexia in metastatic cancer patients. Although limited in its scope, this study also raises the question whether monitoring of PM wasting may serve as a prognostic factor for both cachexia and metastatic extent of the associated cancer, especially in breast cancer.

Acknowledgment

We thank L. Schwartz (Columbia University) for sharing his insights in this study.

Author Contributions

Conceived and designed the experiments: KK, SA. Performed case study patient chart review: NC. Analyzed the data: NC. Wrote the software used for imaging analysis: XG, BZ. Performed histology and pathology: CC, HH. Directed the statistical data analysis: SLP. Wrote the first draft of the manuscript: NC. Contributed to the writing of the manuscript: NC, XG, BZ, CC, SLP, HH, KK, SA. Agreed with manuscript results and conclusions: NC, KK, SA, XG, CC, SLP, HH, BZ. Jointly developed the structure and arguments for the paper: NC, KK, SA. Made critical revisions and approved the final version: NC, KK, SA. All authors read and approved the final manuscript.

Abbreviations

AM: abdominal muscle
BMI: body-mass index
CT: computational tomography
ER: estrogen receptor
IDC: invasive ductal carcinoma
L*n*: *n*th lumbar vertebra
mm^2: millimeters-squared
MRI: magnetic resonance imaging
PM: paraspinal muscle
PR: progesterone receptor
PTHrP: parathyroid hormone related protein
r: Pearson's correlation coefficient
SF: subcutaneous fat
TGF-β: transforming growth factor beta
T*n*: *n*th thoracic vertebra
TU: tumor burden at vertebral spine
VF: visceral fat
ρ: Spearman's correlation coefficient

REFERENCES

1. Kovarik M, Hronek M, Zadak Z. Clinically relevant determinants of body composition, function and nutritional status as mortality predictors in lung cancer patients. *Lung Cancer*. 2014;84(1):1–6.
2. Evans WJ, Morley JE, Argiles J, et al. Cachexia: a new definition. *Clin Nutr*. 2008;27(6):793–9.
3. Tisdale MJ. Mechanisms of cancer cachexia. *Physiol Rev*. 2009;89(2):381–410.
4. Waning DL, Guise TA. Cancer-associated muscle weakness: what's bone got to do with it? *Bonekey Rep*. 2015;4:691.
5. Guttridge DC. A TGF-beta pathway associated with cancer cachexia. *Nat Med*. 2015;21(11):1248–9.
6. Argiles JM, Busquets S, Stemmler B, Lopez-Soriano FJ. Cancer cachexia: understanding the molecular basis. *Nat Rev Cancer*. 2014;14(11):754–62.
7. Fox KM, Brooks JM, Gandra SR, Markus R, Chiou CF. Estimation of cachexia among cancer patients based on four definitions. *J Oncol*. 2009;2009:693458.
8. Chaffer CL, Weinberg RA. A perspective on cancer cell metastasis. *Science*. 2011;331(6024):1559–64.
9. Massague J, Obenauf AC. Metastatic colonization by circulating tumour cells. *Nature*. 2016;529(7586):298–306.
10. Spano D, Heck C, De Antonellis P, Christofori G, Zollo M. Molecular networks that regulate cancer metastasis. *Semin Cancer Biol*. 2012;22(3):234–49.
11. Tisdale MJ. Cancer cachexia. *Curr Opin Gastroenterol*. 2010;26(2):146–151.
12. Waning DL, Guise TA. Molecular mechanisms of bone metastasis and associated muscle weakness. *Clin Cancer Res*. 2014;20(12):3071–7.
13. Fearon KC. Cancer cachexia: developing multimodal therapy for a multidimensional problem. *Eur J Cancer*. 2008;44(8):1124–32.
14. Acharyya S, Oskarsson T, Vanharanta S, et al. A CXCL1 paracrine network links cancer chemoresistance and metastasis. *Cell*. July 6, 2012;150(1):165–78.
15. Zhao B, Colville J, Kalaigian J, et al. Automated quantification of body fat distribution on volumetric computed tomography. *Journal of computer assisted tomography*. Sep–Oct 2006;30(5):777–83.
16. Blum D, Omlin A, Baracos VE, et al. Cancer cachexia: a systematic literature review of items and domains associated with involuntary weight loss in cancer. *Critical reviews in oncology/hematology*. Oct 2011;80(1):114–44.
17. Martin L, Senesse P, Gioulbasanis I, et al. Diagnostic criteria for the classification of cancer-associated weight loss. *Journal of clinical oncology:official journal of the American Society of Clinical Oncology*. January 1, 2015;33(1):90–9.

18. Acerbo AS, Carr GL, Judex S, Miller LM. Imaging the material properties of bone specimens using reflection-based infrared microspectroscopy. *Anal Chem*. 2012;84(8):3607–13.
19. Judex S, Luu YK, Ozcivici E, Adler B, Lublinsky S, Rubin CT. Quantification of adiposity in small rodents using micro-CT. Methods. 2010;50(1):14–9.
20. Martiniova L, Schimel D, Lai EW, Limpuangthip A, Kvetnansky R, Pacak K. In vivo micro-CT imaging of liver lesions in small animal models. *Methods*. 2010;50(1):20–5.
21. Baracos VE, Reiman T, Mourtzakis M, Gioulbasanis I, Antoun S. Body composition in patients with non-small cell lung cancer: a contemporary view of cancer cachexia with the use of computed tomography image analysis. *Am J Clin Nutr*. 2010;91(4):1133S–7S.
22. Kir S, White JP, Kleiner S, et al. Tumour-derived PTH-related protein triggers adipose tissue browning and cancer cachexia. *Nature*. 2014;513(7516):100–4.